








RESEARCH ARTICLE

10.1029/2023JG007967

Magnitude of and Hydroclimatic Controls on CO₂ and CH₄ Emissions in the Subtropical Monsoon Pearl River Basin

Shuai Chen¹, Lishan Ran¹ , Jun Zhong², Boyi Liu¹ , Xiankun Yang³, Ping Yang⁴, Mingyang Tian⁵, Qianqian Yang¹, Si-Liang Li² , Zhifeng Yan² , and Nufang Fang⁶ 

Key Points:

- Seasonal $p\text{CO}_2$ and $p\text{CH}_4$ dynamics in the Pearl River basin were regulated by hydrology and climate
- Mean CO_2 and CH_4 fluxes in the Pearl River basin were $17.8 \text{ Tg C yr}^{-1}$ and $191.5 \text{ Gg C yr}^{-1}$, respectively
- CH_4 evasion in the Pearl River basin was 2.5 times higher than the global mean rate

¹Department of Geography, The University of Hong Kong, Hong Kong, China, ²School of Earth System Science, Institute of Surface-Earth System Science, Tianjin University, Tianjin, China, ³School of Geography and Remote Sensing, Guangzhou University, Guangzhou, China, ⁴School of Geographical Sciences, Fujian Normal University, Fuzhou, China, ⁵Center for Earth System Research and Sustainability (CEN), Institute for Geology, Universität Hamburg, Hamburg, Germany, ⁶Institute of Soil and Water Conservation, Chinese Academy of Sciences and Ministry of Water Resources, Yangling, China

Supporting Information:

Supporting Information may be found in the online version of this article.

Correspondence to:

L. Ran and J. Zhong,
lsran@hku.hk;
jun.zhong@tju.edu.cn

Citation:

Chen, S., Ran, L., Zhong, J., Liu, B., Yang, X., Yang, P., et al. (2024). Magnitude of and hydroclimatic controls on CO₂ and CH₄ emissions in the subtropical monsoon Pearl River basin. *Journal of Geophysical Research: Biogeosciences*, 129, e2023JG007967. <https://doi.org/10.1029/2023JG007967>

Received 15 DEC 2023

Accepted 1 MAY 2024

Abstract Rivers are important ecosystems for carbon emissions and play a crucial role in the global carbon cycle. However, CO₂ and CH₄ emissions from subtropical rivers are substantially under-represented in global-scale estimates. Here, we explored the regional patterns of riverine CO₂ and CH₄ dynamics in the Pearl River basin with a subtropical monsoon climate. We found that its CO₂ and diffusive CH₄ emissions showed a decreasing trend with increasing stream order. Seasonality in CO₂ and diffusive CH₄ emissions was primarily driven by variations in partial pressure of CO₂ ($p\text{CO}_2$) and CH₄ ($p\text{CH}_4$) and gas transfer velocities, which were strongly regulated by hydrology and climate. We further estimated the basin-wide CO₂ and diffusive CH₄ fluxes at $17.8 \pm 7.4 \text{ Tg C yr}^{-1}$ and $191.5 \pm 139.9 \text{ Gg C yr}^{-1}$, respectively. When normalized to the water surface, the mean diffusive fluxes were 790.1 and $8.5 \text{ mmol m}^{-2} \text{ d}^{-1}$ for CO₂ and CH₄, respectively, which were 1.3 and 2.5 times higher than the global mean riverine CO₂ and CH₄ fluxes, respectively. This suggests that the global significance of subtropical rivers is probably underestimated because their substantially higher CH₄ fluxes are unaccounted for. Furthermore, compared with measured $p\text{CO}_2$, the alkalinity-based $p\text{CO}_2$ could introduce significant errors by 20% at ~30% of the sampling sites, underscoring the necessity of direct measurements to reduce uncertainty. This study provides the first estimate of basin-wide CO₂ and diffusive CH₄ emissions in the PRB through direct $p\text{CO}_2$ and $p\text{CH}_4$ measurements, and highlights the role of hydrologic and climatic factors in governing riverine carbon emissions.

Plain Language Summary River systems are important components of the global carbon cycle, releasing large quantities of carbon dioxide (CO₂) and methane (CH₄) into the atmosphere. In this study, we investigated the pattern of dissolved CO₂ and CH₄ concentrations and emissions in the subtropical Pearl River basin in south China. We discovered that the emission rates of both CO₂ and CH₄ decreased with increasing stream order. Seasonal variations in emissions were primarily driven by dissolved CO₂ and CH₄ concentrations as well as the gas transfer velocities across the water-air interface, both of which were strongly regulated by hydrological processes and climatic conditions. We also found that the areal CO₂ and CH₄ emissions were 1.3 and 2.5 times higher, respectively, than the global average. Our study provides the first direct measurement-based estimates of CO₂ and diffusive CH₄ emissions in the Pearl River basin, shedding light on the role of hydrologic and climatic factors in affecting riverine carbon emissions. This research further suggests that the global significance of CH₄ emissions from subtropical river networks may have been substantially underestimated.

1. Introduction

Streams and rivers are increasingly recognized as a dynamic and significant component of the global carbon dioxide (CO₂) and methane (CH₄) emissions (Battin et al., 2023; Raymond et al., 2013; Regnier et al., 2022; Rocher-Ros et al., 2023). Recent studies show that the global emissions of CO₂ and CH₄ were 2.0 Pg C yr^{-1} (Liu et al., 2022) and $20.9 \text{ Tg C yr}^{-1}$ (Rocher-Ros et al., 2023), respectively. However, these estimates are afflicted by large uncertainty, partly due to the limited direct measurements of riverine CO₂ and CH₄ concentrations and the high spatial and temporal heterogeneity in both concentrations and emission (Liu et al., 2022; Raymond et al., 2013; Rocher-Ros et al., 2023). In contrast to lentic waters (e.g., lakes, reservoirs, and ponds), lotic waters

© 2024. The Authors.

This is an open access article under the terms of the [Creative Commons Attribution License](https://creativecommons.org/licenses/by/4.0/), which permits use, distribution and reproduction in any medium, provided the original work is properly cited.

(e.g., streams and rivers) receive less attention in CH₄ dynamics, which is largely because of the persistent conventional perception that well-aerated running waters provide unfavorable conditions for CH₄ generation (Campeau et al., 2014; Stanley et al., 2016). Global CH₄ emissions from freshwater ecosystems were estimated only at 1.1 Tg C yr⁻¹ (Bastviken et al., 2011), which is an order of magnitude lower than the latest estimate (Rocher-Ros et al., 2023). This further suggests that more direct measurements of riverine CH₄ emissions are needed to improve our understanding of global greenhouse gas (GHG) emissions.

There are two methods to measure the surface water CO₂ partial pressure (*p*CO₂) in rivers. The first approach (an indirect method) is based on the thermodynamic relationships for equilibria between carbonate, bicarbonate, and aqueous CO₂, and *p*CO₂ was calculated from pH and alkalinity (Parkhurst & Appelo, 2013). The other approach is through direct measurements using water-air phase equilibration for headspace technique with discrete water samples or infrared gas analyzers to continuously determine the *p*CO₂ (Abril et al., 2015). Although equilibrium equations are more commonly used, the calculated *p*CO₂ is likely overestimated because of the widely distributed acidic, organic-rich streams and rivers, where overestimation could be more than 100% (Abril et al., 2015). This is particularly true for highly polluted Asian rivers with substantial amounts of organic acids being flushed from soils into rivers, a phenomenon that becomes more prominent during the monsoon season (Nayna et al., 2021). Moreover, the accuracy of the indirect method-based *p*CO₂ relies highly on pH. Uncertainties of the calculated *p*CO₂ can reach up to ±21% when the field measurements have uncertainties of ±0.1 pH units (Marx et al., 2017). These uncertainties stress the importance of conducting direct measurements of *p*CO₂ in inland waters. However, the *p*CO₂ determined from headspace equilibrium can also lead to a high systematic error (up to -300%) if the chemical equilibration of the carbonate system is not properly considered, especially for waters that are highly undersaturated but equilibrated with ambient air (Koschorreck et al., 2021). Consequently, many river ecosystems worldwide still lack credible data on *p*CO₂, and little is known about the errors introduced by the alkalinity-based *p*CO₂. Owing to the large spatial and temporal variabilities of the *p*CO₂ and the complex physicochemical characteristics of aquatic environment (Ran et al., 2021; Raymond et al., 2013), studies on *p*CO₂ in both headwater streams and large rivers should be conducted to strengthen our mechanistic understanding of the differences between alkalinity-based and headspace-based *p*CO₂ across the full range of river and stream networks.

Subtropical regions are characterized by more pronounced seasonal differences between summer (hot and humid) and winter (cool and dry) than tropical regions (Sawakuchi et al., 2014; Yao et al., 2007). Moreover, compared with temperate rivers, the higher temperature in subtropical rivers provides a suitable condition for methanogenesis (Yvon-Durocher et al., 2014) and facilitates increased input of terrestrial CO₂ as a result of enhanced primary productivity (Liu et al., 2021), making subtropical rivers potential hotspots for GHG emissions. With these contrasting hydrologic and climatic conditions, subtropical rivers function as unique ecosystems for GHG emissions in the global context. However, research on CH₄ dynamics in subtropical river ecosystems has received much less attention compared with rivers in other latitudes (Stanley et al., 2023). Furthermore, direct measurements of *p*CO₂ in subtropical rivers are particularly underrepresented in East Asia when compared with other regions (Liu et al., 2022). East Asia has been one of the most rapidly urbanizing regions in the world over the past few decades, where agricultural and urban-impacted rivers are likely potent GHG emitters (Park et al., 2018). Besides, large quantities of anthropogenic nutrients, coupled with increased nutrient residence time due to dam operation, have substantially enhanced the aquatic primary productivity in East Asia (Han et al., 2018; Park et al., 2018).

The Pearl River is a large subtropical river in South China and the second-largest river entering the South China Sea. The Pearl River basin (PRB) is currently undergoing a series of environmental problems (e.g., water pollution) followed by rapid urbanization and industrialization (Zhang et al., 2009). Although the CO₂ dynamics in the Pearl River have long been reported (Liu & Han, 2021; Yao et al., 2007; Zhang et al., 2009), they were all based on calculated *p*CO₂ with large uncertainty. To our knowledge, direct measurements of *p*CO₂ were only reported in two low-gradient streams (Zhang, Li, et al., 2017; Zhang et al., 2021), the Dongjiang River (a tributary of the Pearl River; Liu et al., 2021), and the Pearl River Estuary (Guo et al., 2009). In comparison, studies on CH₄ emissions were restricted to the Pearl River Estuary (Ye et al., 2019). A comprehensive study of the magnitude of CO₂ and CH₄ emissions based on direct measurements in the subtropical monsoon PRB remains poorly explored. In this study, we present the first integrated study of CO₂ and CH₄ concentrations and emissions from the subtropical PRB spanning eight Strahler stream orders. The specific objectives were to: (a) explore the spatial and seasonal patterns of CO₂ and CH₄ concentrations and emissions at the basin scale, (b) assess the reliability of the calculated *p*CO₂ using the alkalinity-based method in the study area, and finally, (c) estimate the basin-wide CO₂

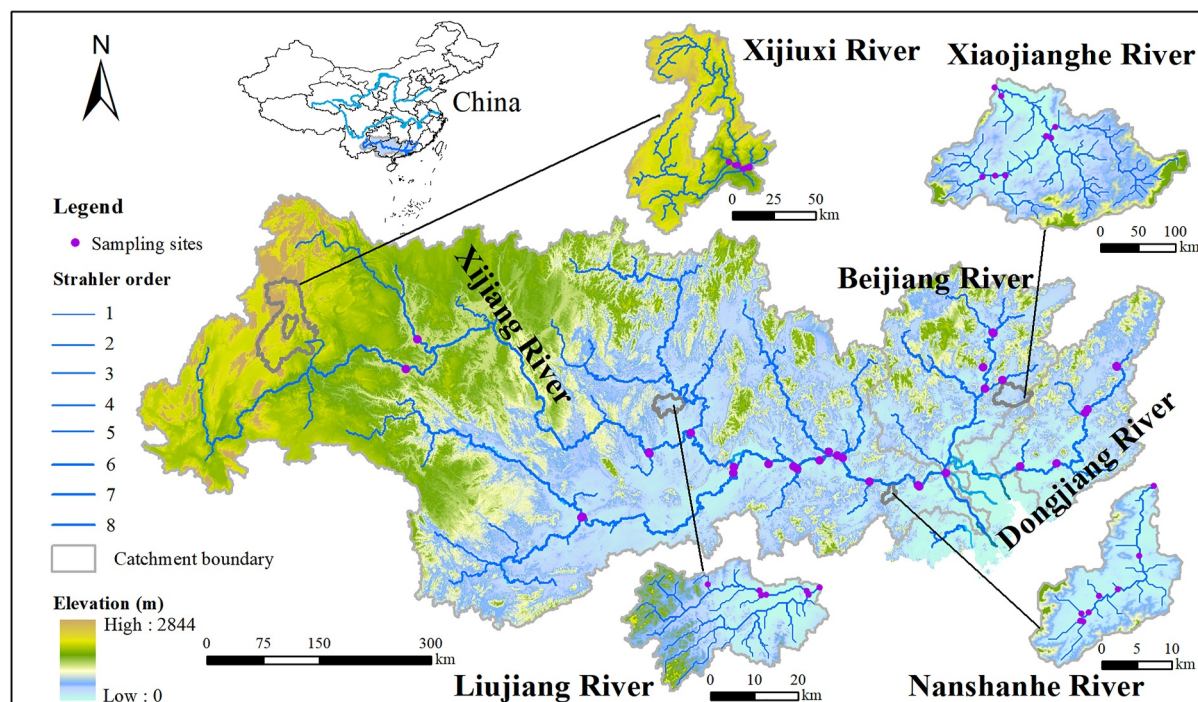


Figure 1. Location of the sampling sites ($n = 62$) in headwater streams (Nanshanhe River, Liujiang River, Xijiuxi River, and Xiaojianghe River) and along large rivers (the Xijiang River, Beijiang River, and Dongjiang River) of the Pearl River basin. See Table S1 in Supporting Information S1 for more information.

and diffusive CH_4 fluxes in the PRB and derive their biogeochemical implications for subtropical riverine CO_2 and CH_4 dynamics. Our study provides the first basin-wide observations showing the CO_2 and diffusive CH_4 emissions in the large subtropical monsoon PRB and sheds light on the global significance of CH_4 emissions from subtropical streams and rivers.

2. Materials and Methods

2.1. Study Area

The Pearl River is the second-largest river in terms of annual discharge and the third-longest river in China, with a drainage area of $4.53 \times 10^5 \text{ km}^2$ and eight Strahler orders (Figure 1). There are three large tributaries, including the Xijiang, Beijiang, and Dongjiang rivers, located in the west, north, and east of the PRB, respectively. The relief in the PRB is generally high in the northwest and low in the southeast, with the altitude ranging from ~ 0 to 2,800 m (Figure 1; Table S1 in Supporting Information S1). Carbonate rocks are widely distributed in the PRB, especially in the Xijiang River (Table S1 in Supporting Information S1). The upper reach of the Xijiang River is located in the Southeast Asia Karst Region, the world's largest karst area. The PRB is highly affected by monsoons, with about 80% of the annual precipitation falling in the rainy season (April–December). The annual average temperature ranges from 14°C to 22°C , and the annual average precipitation varies in the range of 1,200–2,200 mm across the PRB (Han et al., 2018).

Forest is the dominant land use in the PRB, followed by cropland and grassland (Table S1 in Supporting Information S1). The lower reaches of the three tributaries are mainly located in Guangdong Province, one of the most economically developed regions in China, and are all predominated by urban land uses. In comparison, agricultural land use is prevalent in the upper and middle reaches of the Xijiang River. Reservoirs and dams have been widely constructed in the PRB, especially in the Xijiang River basin that has more than 230 large reservoirs (Han et al., 2018).

The lithology, land use, and elevation also vary substantially in the four studied headwater streams (i.e., the Nanshanhe (NSH), Liujiang (LJ), Xijiuxi (XJX), and Xiaojianghe (XJH) rivers; Figure 1; Table S2 in Supporting Information S1). Of these headwater streams, carbonate rocks and mixed sedimentary rocks are mainly

distributed in the XJX and LJ watersheds, whereas the NSH and XJH watersheds are primarily underlain by acid plutonic rocks, metamorphics, and carbonate rocks. While agricultural and grassland uses are the major land use types in the XJX watershed, agriculture and forest are the major land use types in the other three watersheds. In addition, urban land use is also important for the LJ and NSH watersheds.

2.2. Sampling Strategy and Geospatial Analyses

Sixty-two tributary and mainstem sites covering all the eight Strahler orders of the PRB were sampled from July 19th to August 3rd (wet season) and December 7th to 22nd (dry season) of 2021. These widely distributed streams across the PRB were carefully chosen to reflect the spatial heterogeneity in topography, lithology, hydrology, and land cover within and among regions. Of the 62 sampling sites, 31 sites are located in the mainstream and main tributaries of the Pearl River (Strahler orders 5–8), and the remaining 31 sites are distributed in four small watersheds (Strahler orders 1–5; Figure 1). Delineation of individual sub-watersheds upstream of the sampling sites and estimation of their drainage area (range: 6–308,178 km²; Table S1 in Supporting Information S1) were achieved through a Digital Elevation Model (DEM) with a 30 m resolution (ASTER v3 DEM, NASA et al., 2018) using the spatial analyst tools of ArcGIS 10.2. Stream networks were obtained from the HydroSHEDS database (Linke et al., 2019). The distribution of physiographic characteristics (e.g., lithology and land cover) of the study watersheds was calculated from published geospatial data and delineated sub-watersheds (see details in Table S1 in Supporting Information S1).

2.3. Field Sampling and Laboratory Analysis

During the two sampling campaigns, 124 water samples were collected from the middle of streams or from the river bank if the middle is inaccessible. All sampling sites were far away from any visible sewage pollution. River water $p\text{CO}_2$ and $p\text{CH}_4$ were measured by the headspace equilibrium method (see details in Supporting Information S1; Campeau et al., 2014). The theoretical $p\text{CO}_2$ was also determined from pH, water temperature (WT), and alkalinity using PHREEQC version 3 (Parkhurst & Appelo, 2013). The areal emission rate of CO_2 ($F\text{CO}_2$) and CH_4 ($F\text{CH}_4$) was calculated using a 9.3 L floating chamber at 8 min intervals (0, 8, 16, 24, 32, and 40 min) by collecting 60 mL of gas from the chamber through a syringe and stored in 12-mL Exetainer vials. The rate of gas concentration change within the chamber was utilized to determine the $F\text{CO}_2$ and $F\text{CH}_4$ (Equation S2 in Supporting Information S1; see details in Supporting Information S1).

At each sampling site, we measured WT, dissolved oxygen (DO), pH, and electrical conductivity (EC) using a portable multiparameter probe (Multi 3,420, WTW GmbH, Germany). The pH probe was calibrated using standard pH buffers (4.01, 7.00, and 10.01) prior to measurement, and triple measurements demonstrated a precision of ± 0.01 pH units. In addition, alkalinity was determined through triplicate end-point titrations in the field, utilizing 0.02 mol L⁻¹ hydrochloric acid and a mixed indicator comprising bromocresol green and methyl red. More detailed information on water chemistry was described in Supporting Information S1. Wind speed and atmospheric pressure were measured by a handheld anemometer (Kestrel 2500, USA) at 1.5 m above the water surface. Flow velocity was measured using a water flow probe (FP111, USA) with a precision of 0.1 m s⁻¹. Stream width was measured by a laser rangefinder, and water depth was measured by a sonar fathometer. Sediment grades of the riverbed at each site were recorded following the classification method of Valentine (2019), which includes mud, sand, and gravel.

2.4. Basin-Scale Estimation of Annual CO_2 and Diffusive CH_4 Fluxes

The water surface area of the PRB in the wet and dry seasons was determined by multiplying the measured mean stream width with the corresponding stream length derived from the HydroSHEDS database (Linke et al., 2019) for each Strahler order (orders 1–8). To avoid underestimating the stream length by missing the smallest streams, the length of Strahler order 0 streams was estimated by extrapolating the exponential correlation (Figure S1a in Supporting Information S1) between stream order and stream length (Liu et al., 2023; Raymond et al., 2013). The stream width of Strahler order 0 streams was estimated using the same method as the stream length (Figures S1b and S1c in Supporting Information S1). Although intermittent streams play a disproportionately important role in CO_2 emissions (Gómez-Gener et al., 2021), these streams were not considered in this study. The flux error arising from ignoring these intermittent streams is likely minimal because part of the surface area of these intermittent

streams has been included in Strahler order 0 streams. Meanwhile, the abundance of intermittent streams in subtropical regions with high runoff, such as the PRB, is relatively small (Liu et al., 2022).

The areal emission rates of diffusive CO₂ and CH₄ in each Strahler order stream were calculated based on the measured *p*CO₂, *p*CH₄, and gas transfer velocities (*k*), which were converted from the standardized gas transfer velocity (*k*₆₀₀) using the empirical model (Equations S3–S5 in Supporting Information S1; Raymond et al., 2012). These rates were then combined with our estimated water surface area of each stream order to calculate the total fluxes of diffusive CO₂ and CH₄ during the wet and dry seasons in the PRB (Equations S6 and S7 in Supporting Information S1; see details in Supporting Information S1).

Contrary to CO₂, diurnal variations in CH₄ emissions were not considered in this study due to the lack of studies on a large spatial scale (see details in Supporting Information S1). The total CO₂ and diffusive CH₄ fluxes were normalized to the water surface area and landscape area to calculate the area-weighted fluxes. We also calculated the CO₂ equivalents (CO₂-eq) of CH₄ by assuming that CH₄ has a 28 times stronger global warming potential than CO₂ over a 100-year period (Ciais et al., 2014). Uncertainties in CO₂ and CH₄ emission fluxes were determined using Monte Carlo simulations that ran 10,000 iterations. The Monte Carlo analysis was conducted for streams grouped by Strahler orders and sampling seasons, considering the uncertainties associated with riverine *p*CO₂ and *p*CH₄, *k* values, and water surface area. During each iteration, parameters were randomly resampled from normal distributions constrained by the mean and standard deviation (SD). The uncertainties obtained from the Monte Carlo analysis were reported as the 1δ deviation of the simulated emission magnitude distributions.

2.5. Statistical Analysis

The Shapiro-Wilk test was used to examine the normality of the data. One-way ANOVA with Tukey's post-test, Mann-Whitney U test, and Kruskal-Wallis test followed by Holm's Stepdown Bonferroni correction were performed for comparison of distributions between two or multiple groups by using SPSS 26. Simple linear regressions were applied using Origin (Pro) 2021 to assess the relationship between measured *p*CO₂ and alkalinity-based calculated *p*CO₂, predict the calculation error of *p*CO₂ using pH, and explore the correlations between *p*CO₂, *p*CH₄, WT, and DO. Values are presented as median ± SD. All statistical tests were carried out at a 0.05 significance level. Because aquatic CO₂ and CH₄ concentrations and fluxes would be greatly influenced by outliers, median values are a better choice to represent the data range rather than means (Hutchins et al., 2019; Stanley et al., 2023).

3. Results

3.1. Spatial and Temporal Variations in Water Quality Variables

The water temperature varied from 20.0 to 35.3°C with a median of 30.1°C in the wet season and from 13.4 to 21.2°C with a median of 18.2°C in the dry season (Table 1). In general, river water was mildly alkaline, with the pH increasing from 6.66 to 8.92 (median: 7.77) in the wet season and from 6.53 to 8.51 (median: 7.92) in the dry season. Conductivity was slightly higher during the dry season, with a median of 286 and 295 μS cm⁻¹ for the wet and dry seasons, respectively. Alkalinity was similar in both seasons but varied in a wide range (varied from 359 to 3,838 μmol L⁻¹ with a median of 2,040 μmol L⁻¹ in the wet season and from 483 to 4,385 μmol L⁻¹ with a median of 2,113 μmol L⁻¹ in the dry season). All sites were significantly less oxygenated in the wet season (median: 7.0 mg L⁻¹) than in the dry season (median: 9.1 mg L⁻¹).

3.2. Spatial and Temporal Variations in Riverine CO₂ and CH₄ Dynamics

The riverine *p*CO₂ in the wet season varied from 146 to 6,362 μatm with a median of 2,789 μatm (*n* = 62), which is significantly higher than the *p*CO₂ level in the dry season (median: 1,351 μatm; *p* < 0.01; Table 1). In total (*n* = 124), approximately 97% of the measurements had the *p*CO₂ higher than the atmospheric equilibrium (~414 μatm). Samples with *p*CO₂ lower than the atmospheric equilibrium were all super-saturated in DO (i.e., higher than 100%), and the sampling sites are all located within 15 km downstream of dams. The riverine *p*CH₄ in all streams was higher than the atmospheric *p*CH₄ (~1.87 μatm). The *p*CH₄ varied by four orders of magnitude, ranging from 14 to 11,119 μatm (a highly polluted urban stream in the LJ catchment), with a median of 495 μatm in the wet season. In comparison, the median *p*CH₄ in the dry season (168 μatm) was substantially lower than the wet season.

Table 1
Water Chemistry Characteristics of the Study Streams and Rivers in the PRB

Parameter	Units	Xijiang (n = 42)				Beijiang (n = 14)				Dongjiang (n = 6)				All	p values
		Wet season	Dry season	Dry season	Wet season	Wet season	Dry season	Dry season	Wet season	Wet season	Dry season	Dry season	Wet season		
Water Temperature	°C	28.9 (20.0–33.1)	18.6 (14.0–21.2)	32.3 (28.3–35.3)	17.1 (13.4–19.3)	32.8 (30.4–34.3)	17.1 (13.4–19.3)	30.1 (20.0–35.3)	18.2 (13.4–21.2)	7.92 (6.53–8.51)	7.92 (6.53–8.51)	7.92 (6.53–8.51)	7.92 (6.53–8.51)	18.2 (13.4–21.2)	<0.0001
pH		7.83 (7.04–8.28)	8.11 (6.53–8.51)	7.38 (6.66–8.92)	7.47 (6.84–8.48)	7.52 (7.30–8.35)	7.59 (7.34–7.74)	7.77 (6.66–8.92)	7.92 (6.53–8.51)	7.92 (6.53–8.51)	7.92 (6.53–8.51)	7.92 (6.53–8.51)	7.92 (6.53–8.51)	7.92 (6.53–8.51)	<0.0001
Conductivity	µS cm ⁻¹	346 (104–772)	362 (175–146)	176 (62–384)	270 (89–655)	148 (130–242)	178 (105–225)	286 (62–772)	295 (89–746)	295 (89–746)	295 (89–746)	295 (89–746)	295 (89–746)	0.13	
Alkalinity	µmol L ⁻¹	2,548 (792–3,838)	2,660 (483–4,385)	736 (359–1,671)	1,054 (555–2,420)	831 (573–1,083)	803 (607–1,219)	2,040 (359–3,838)	2,113 (483–4,385)	2,113 (483–4,385)	2,113 (483–4,385)	2,113 (483–4,385)	2,113 (483–4,385)	0.36	
Oxygen	mg L ⁻¹	7.0 (1.8–8.3)	9.1 (4.5–12.2)	7.1 (5.5–10.4)	9.6 (2.1–11.2)	6.8 (5.0–9.7)	8.7 (8.0–9.1)	7.0 (1.8–10.4)	9.1 (2.1–12.2)	9.1 (2.1–12.2)	9.1 (2.1–12.2)	9.1 (2.1–12.2)	9.1 (2.1–12.2)	<0.0001	
Oxygen Saturation	%	94.6 (23.0–109.6)	101.5 (48.2–144.5)	99.9 (78.2–150.1)	97.6 (21.9–115.4)	96.2 (72.9–130.4)	91.6 (85.0–95.1)	96.4 (23.0–150.1)	99.6 (21.9–144.5)	99.6 (21.9–144.5)	99.6 (21.9–144.5)	99.6 (21.9–144.5)	99.6 (21.9–144.5)	0.08	
<i>k</i> ₆₀₀	m d ⁻¹	1.3 (0.3–9.8)	0.6 (0.1–5.1)	0.6 (0.4–4.3)	1.0 (0.3–3.4)	0.8 (0.4–4.2)	0.5 (0.3–0.9)	1.1 (0.3–9.8)	0.6 (0.1–5.1)	0.6 (0.1–5.1)	0.6 (0.1–5.1)	0.6 (0.1–5.1)	0.6 (0.1–5.1)	<0.01	
<i>p</i> CO ₂	µatm	2,710 (974–6,362)	1,235 (439–8,708)	3,151 (146–5,348)	1,547 (387–4,831)	1,950 (273–4,630)	1,237 (976–1,442)	2,789 (146–6,362)	1,351 (387–8,708)	1,351 (387–8,708)	1,351 (387–8,708)	1,351 (387–8,708)	1,351 (387–8,708)	<0.0001	
<i>p</i> CH ₄	µatm	496 (20–11,119)	156 (43–9,596)	454 (14–3,545)	168 (68–3,907)	1,468 (271–6,203)	227 (87–583)	495 (14–11,119)	168 (43–9,596)	168 (43–9,596)	168 (43–9,596)	168 (43–9,596)	168 (43–9,596)	<0.0001	
<i>F</i> CO ₂	mmol m ⁻² d ⁻¹	97.0 (18.5–1,231.2)	20.7 (–6.6–198.5)	76.1 (–16.3–561.0)	40.3 (–2.5–281.0)	58.0 (–25.7–220.4)	14.3 (6.0–16.1)	91.7 (–25.7–1,231.2)	20.6 (–20.5–281.0)	20.6 (–20.5–281.0)	20.6 (–20.5–281.0)	20.6 (–20.5–281.0)	20.6 (–20.5–281.0)	<0.0001	
<i>F</i> CH ₄	mmol m ⁻² d ⁻¹	0.78 (0.06–120.95)	0.20 (0.02–3.79)	0.93 (0.27–18.75)	0.19 (0.03–24.72)	3.25 (0.16–49.89)	0.16 (0.05–0.31)	0.84 (0.06–120.95)	0.19 (0.02–24.72)	0.19 (0.02–24.72)	0.19 (0.02–24.72)	0.19 (0.02–24.72)	0.19 (0.02–24.72)	<0.0001	

Note. Values were presented as median (min-max). The p values were provided to indicate the seasonal differences across all samples using the Mann-Whitney U test.

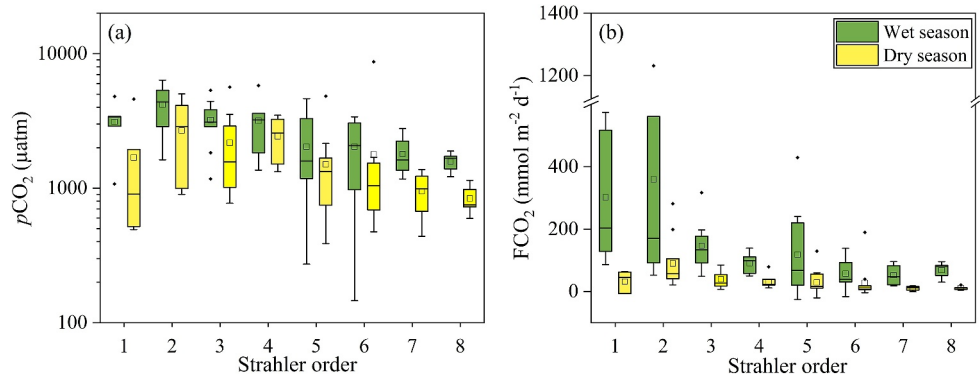


Figure 2. Box-and-whisker plots showing (a) $p\text{CO}_2$ and (b) CO_2 emission rate ($F\text{CO}_2$) by Strahler order in the wet and dry seasons. The box represents the 25th and 75th percentiles, the open square and horizontal line represent the mean and median, respectively, and the whiskers represent 1.5 times the upper and lower interquartile ranges (IQR). The solid dots denote outliers.

Riverine CO_2 fluxes were significantly higher ($p < 0.001$) in the wet season (ranged from -25.7 to $1,231.2 \text{ mmol m}^{-2} \text{ d}^{-1}$ with a median of $91.7 \text{ mmol m}^{-2} \text{ d}^{-1}$) than in the dry season (ranged from -20.5 to $281.0 \text{ mmol m}^{-2} \text{ d}^{-1}$ with a median of $20.6 \text{ mmol m}^{-2} \text{ d}^{-1}$). Similar to CO_2 fluxes, diffusive CH_4 fluxes were also significantly higher in the wet season ($p < 0.01$; median: $0.84 \text{ mmol m}^{-2} \text{ d}^{-1}$) than in the dry season (median: $0.19 \text{ mmol m}^{-2} \text{ d}^{-1}$) and varied widely from 0.06 to $120.95 \text{ mmol m}^{-2} \text{ d}^{-1}$ in the wet season and from 0.02 to $24.72 \text{ mmol m}^{-2} \text{ d}^{-1}$ in the dry season.

There was a decreasing trend of $p\text{CO}_2$ and $F\text{CO}_2$ with increasing stream order (especially for stream orders 2–7; Figure 2). Second-order streams exhibited the highest median $p\text{CO}_2$ at $4,377$ and $2,881 \text{ µatm}$ in the wet and dry seasons, respectively. The median $p\text{CO}_2$ gradually decreased to $1,669$ and 752 µatm in the eighth-order streams in the wet and dry seasons, respectively. In contrast, $p\text{CH}_4$ and $F\text{CH}_4$ showed no discernible trend with stream order (Figure 3). However, similar to CO_2 , the second order streams exhibited the highest $p\text{CH}_4$ and $F\text{CH}_4$, with a median of $1,858$ and 522 µatm for the $p\text{CH}_4$ in the wet and dry seasons, respectively, and a median of 19.78 and $1.19 \text{ mmol m}^{-2} \text{ d}^{-1}$ for the $F\text{CH}_4$ in the wet and dry seasons, respectively. We also found a gradual decrease of $p\text{CO}_2$ with increasing stream width in both seasons (Figures S2a and S2b in Supporting Information S1), but there was no significant trend between $p\text{CH}_4$ and stream width (Figures S2c and S2d in Supporting Information S1). Additionally, stream water $p\text{CH}_4$ did not show significant differences across various sediment grades (Figure 4). Furthermore, there were weak but significantly positive correlations between WT and stream water $p\text{CO}_2$ and $p\text{CH}_4$ ($p < 0.0001$; Figures 5a and 5b). In comparison, DO was significantly negatively correlated with $p\text{CO}_2$ and $p\text{CH}_4$ ($p < 0.0001$; Figures 5c and 5d).

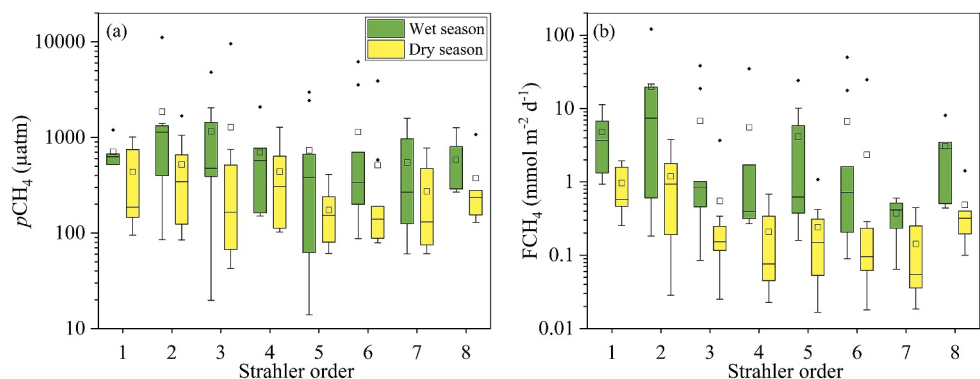


Figure 3. Box-and-whisker plots showing (a) $p\text{CH}_4$ and (b) diffusive CH_4 emission rate ($F\text{CH}_4$) by Strahler order in the wet and dry seasons. The box represents the 25th and 75th percentiles, the open square and horizontal line represent the mean and median, respectively, and the whiskers represent 1.5 times the upper and lower interquartile ranges (IQR). The solid dots denote outliers.

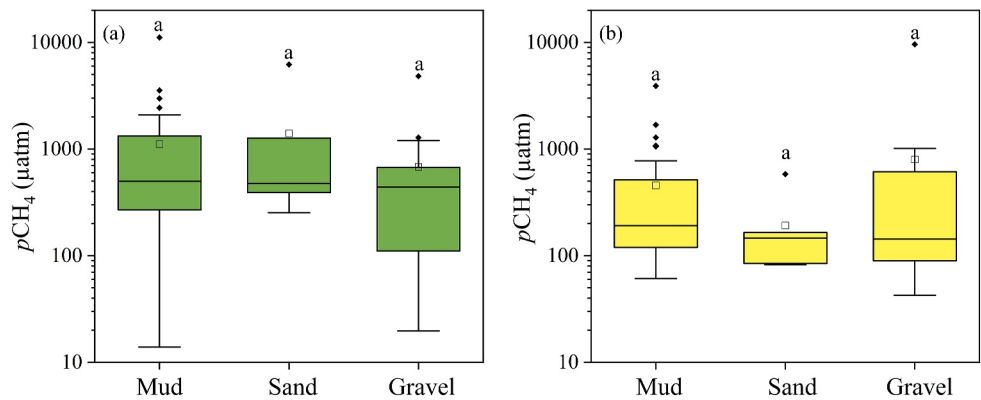


Figure 4. Box-and-whisker plots showing the $p\text{CH}_4$ by sediment grades in the (a) wet season and (b) dry season. The box represents the 25th and 75th percentiles, the open square and horizontal line represent the mean and median, respectively, and the whiskers represent 1.5 times the upper and lower interquartile ranges (IQR). The solid dots denote the outliers. The letters above the boxes represent significant differences between the grouping of sediment grades at the significance level of 0.05.

3.3. Comparison Between Headspace-Based $p\text{CO}_2$ and Alkalinity-Based $p\text{CO}_2$

The slope of the linear regression between headspace-based $p\text{CO}_2$ and modeled $p\text{CO}_2$ using alkalinity was 1.02 for all samples ($n = 124$; Figure 6a). The mean ratio between modeled to measured $p\text{CO}_2$ was 0.95 (± 0.20 ; Figure 6b). For individual sites, however, the ratio varied widely in the range of 0.37–1.53. In total, 28% of the modeled $p\text{CO}_2$ values showed underestimation or overestimation of more than 20%. A greater magnitude of underestimation tends to occur when river water pH is higher than 8 (Figure 6b).

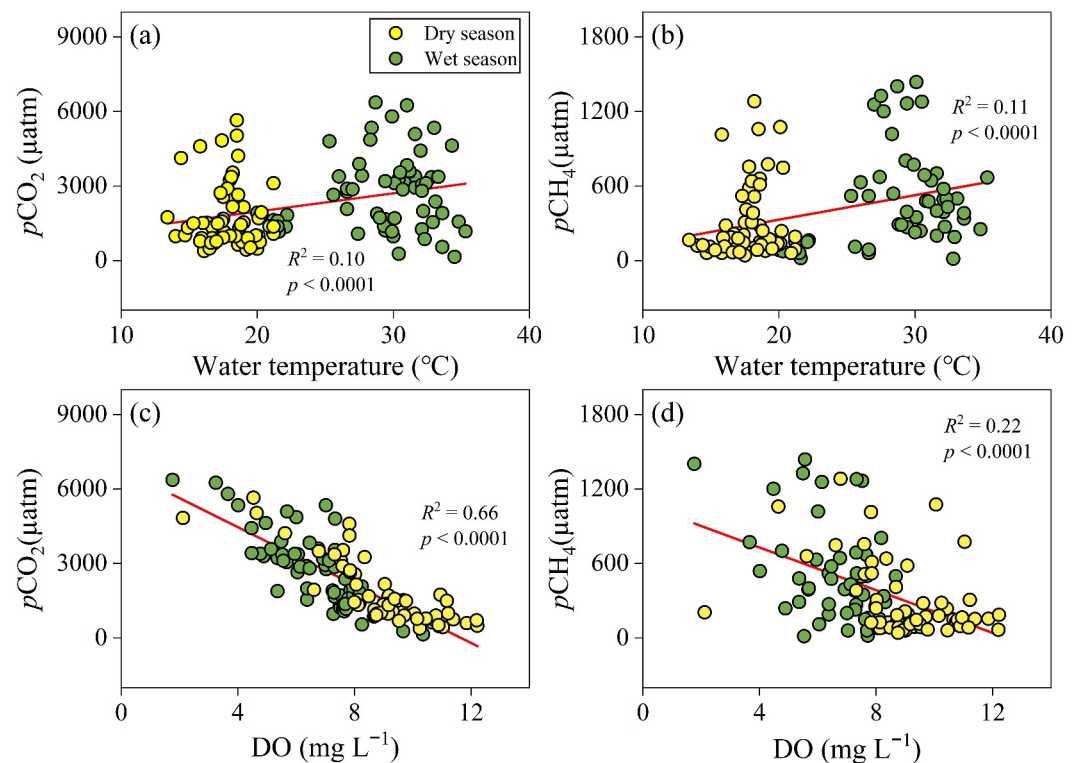


Figure 5. Stream water $p\text{CO}_2$ and $p\text{CH}_4$ as a function of (a, b) water temperature and (c, d) dissolved oxygen (DO). Outliers, values that are $1.5 \times \text{IQR}$ greater than the third quartile, were excluded from linear regression analyses (solid red line).

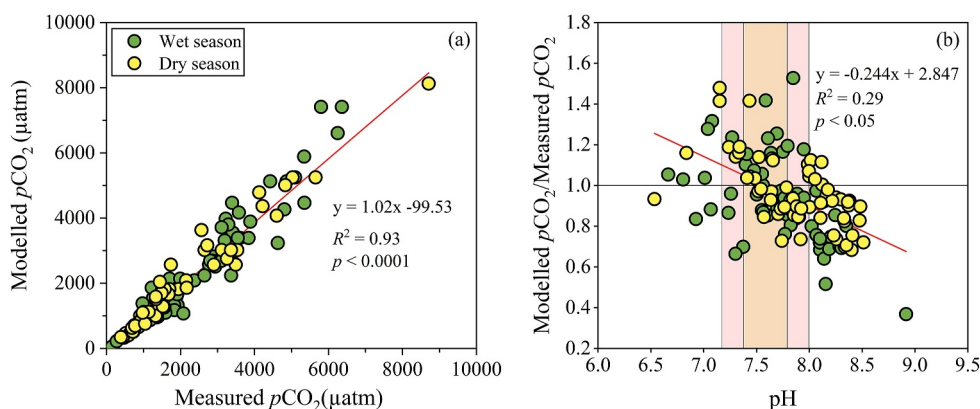


Figure 6. (a) Comparison between measured $p\text{CO}_2$ based on the headspace method and modeled $p\text{CO}_2$ using alkalinity, (b) pH as a good indicator to constrain the error of modeled $p\text{CO}_2$, as shown by the ratio of modeled and measured $p\text{CO}_2$ versus pH. The black horizontal line in panel (b) represents the ratio of 1, and the baby pink and navajo-white bands represent the 90% and 95% precision of the estimates, respectively.

3.4. Basin-Wide Estimates of CO_2 and Diffusive CH_4 Fluxes

The water surface area of the stream network in the PRB was 5,220 km^2 in the wet season and 5,063 km^2 in the dry season (Figure S3 in Supporting Information S1). Total riverine CO_2 emissions were estimated at $17.8 \pm 7.4 \text{ Tg C yr}^{-1}$, with CO_2 emission during the wet season ($14.2 \pm 6.4 \text{ Tg C}$) nearly three times higher than that in the dry season ($4.8 \pm 3.3 \text{ Tg C}$). Moreover, the total riverine CH_4 emissions were estimated to be $191.5 \pm 139.9 \text{ Gg C yr}^{-1}$, with the CH_4 emission fluxes in the wet and dry seasons at $158.8 \pm 139.2 \text{ Gg C}$ and $46.5 \pm 27.6 \text{ Gg C}$, respectively. When expressed as CO_2 -equivalents, the total flux was $23.2 \text{ Tg CO}_2\text{-eq yr}^{-1}$, with a dominant contribution from CO_2 (77%). The $F\text{CO}_2/F\text{CH}_4$ ratio (in $\text{CO}_2\text{-eq}$), varying from 1.8 to 4.9, does not exhibit any detectable trend with stream order (Figure 7). When normalized to the water surface area, the diffusive fluxes were 790.1 and 8.5 $\text{mmol m}^{-2} \text{ d}^{-1}$ for CO_2 and CH_4 , respectively. Similar to the in situ measured CO_2 fluxes, the extrapolated CO_2 fluxes in the PRB showed a decreasing trend with increasing stream order (Figure 7). Consequently, headwater streams (0–2) contributed to 75% of the total CO_2 fluxes, despite that they accounted for only 31% of the total water surface area. In contrast to the in situ measured diffusive CH_4 fluxes, the extrapolated

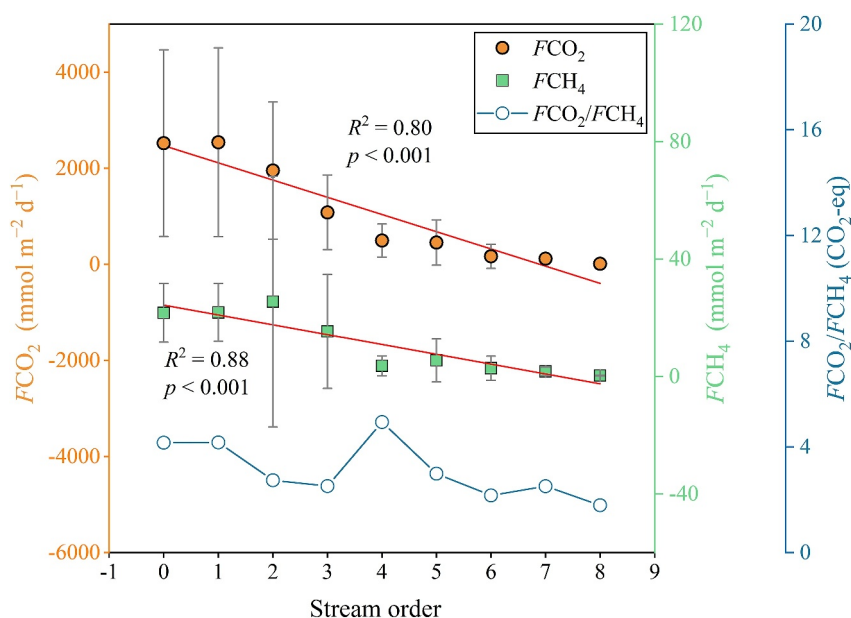


Figure 7. Decreasing $F\text{CO}_2$, $F\text{CH}_4$, and $F\text{CO}_2/F\text{CH}_4$ ratio (in $\text{CO}_2\text{-eq}$) with increasing stream order. $F\text{CO}_2$ and $F\text{CH}_4$ were shown as mean \pm SD.

diffusive CH₄ fluxes also significantly decreased with increasing stream order ($R^2 = 0.85$, $p < 0.0001$), with headwater streams (0–2) contributing to 72% of the total diffusive CH₄ fluxes.

4. Discussion

4.1. Spatial Patterns in CO₂ and CH₄ Concentrations and Fluxes

Riverine $p\text{CO}_2$ is typically highest in headwater streams where hydrological flow paths are well connected with CO₂-rich groundwaters and riparian soils (Marx et al., 2017). The high $p\text{CO}_2$ in headwater streams, coupled with fast gas transfer velocities in mountainous regions, resulted in rapid CO₂ outgassing and thus the high $f\text{CO}_2$ in low-order streams and the decreasing $p\text{CO}_2$ along the river course (Figure 2). This is consistent with previous studies conducted in other climatic regions (e.g., Butman & Raymond, 2011; Campeau et al., 2014; Hutchins et al., 2019; Ran et al., 2021) and the Yangtze River (Ran et al., 2017), which shares a similar subtropical monsoon climate as the PRB. Notably, the $p\text{CO}_2$ levels remained relatively constant in downstream large rivers (i.e., Strahler order 6–8) located in the lower reaches of the Yangtze River Basin that flow through the low-gradient landscapes (Ran et al., 2017). However, even in the lower reaches of the PRB, the $p\text{CO}_2$ in large rivers (i.e., Strahler order 6–8) exhibited a decreasing trend as the stream order increased (Figure 2). This trend is likely caused by the gradual reduction in river-groundwater hydrological connectivity, which can be attributed to the prevalence of mountains and hills across the PRB (Figure 1). These mechanisms that lead to the decreasing $p\text{CO}_2$ and $f\text{CO}_2$ with stream order can also explain the declining $p\text{CO}_2$ with increasing stream width (Figure S2 in Supporting Information S1). Apart from the influence of hydrological conditions, nutrient availability probably also contributed to the decreasing trend of $p\text{CO}_2$ with increasing stream order. Both dissolved total nitrogen (TN) and total phosphorus (TP) exhibited a decreasing trend with increasing stream order in both the wet and dry seasons (Figures S4a and S4b in Supporting Information S1), and a similar trend for dissolved organic carbon (DOC) displayed in the wet season (Figure S4c in Supporting Information S1). Higher nutrient and DOC loading can enhance the production of GHGs (Park et al., 2023) in lower-order streams, illustrating the anthropogenic impact on GHG emissions, as evidenced by the positive correlation between catchment population density and $p\text{CO}_2$, as well as $p\text{CH}_4$ (Figure S5 in Supporting Information S1).

In contrast to $p\text{CO}_2$, there were no apparent changes in $p\text{CH}_4$ with stream order and stream width (Figure 3 and Figure S2 in Supporting Information S1), despite the fact that higher nutrient supply and relatively lower DO levels in lower-order streams (Figure S6 in Supporting Information S1) provide a favorable environment for CH₄ production. However, this does not imply that the spatial distribution of $p\text{CH}_4$ was not affected by anthropogenic activities (Figure S5b in Supporting Information S1). This is likely due to the high coverage extent of and connectivity with wetlands (Figure S7 in Supporting Information S1), which is generally associated with high CH₄ concentrations (Borges et al., 2019; Zhang, Zimmermann, et al., 2017). Consequently, higher-order streams tend to exhibit high CH₄ production rates, potentially masking any decreasing trend of $p\text{CH}_4$ with stream order. The differences in the distribution patterns of CO₂ and CH₄ indicate that the controlling mechanisms of the two gases were different. Although both gases share the same sources from soils, groundwater (Lupon et al., 2019), and the processing of organic matter (Campeau & Del Giorgio, 2014), dissolved CO₂ is primarily regulated by the pH-dependent reaction equilibrium among inorganic carbon species (Marx et al., 2017; Stets et al., 2017). This pH-related effect is known as carbonate buffering, and it is most pronounced in waters with high alkalinity (Stets et al., 2017), such as karst rivers in the PRB. Moreover, CH₄ emissions did not show significantly higher fluxes at sites with fine sediment (Figure 4) as previously reported (e.g., Sawakuchi et al., 2014; Tang et al., 2021). A large volume of fine sediment deposits in the streambed can create an anoxic habitat conducive to methane production (Zhu et al., 2022), and the delivery of fine sediment has been found to be closely correlated with increases in riverine DOC induced by anthropogenic activities, further supporting the heightened methane emissions (e.g., Tang et al., 2021; Zhu et al., 2022). However, we did not find significant differences in riverine DOC concentrations among the three sediment grades (figure not shown), resulting in the insignificant effect of fine sediment on increasing CH₄ emissions in the PRB. This was also likely due to the large spatial variability of landscapes across the PRB that drives great changes in gas transfer velocities and methane production rates (Crawford et al., 2017; Hutchins et al., 2019), thereby masking the impacts of sediment grade.

The PRB spans a wide range of landscape features (e.g., land use types/covers, lithology, and elevation) and climate, which results in significant differences in water chemistry and CO₂ and CH₄ dynamics (Table 1). The median riverine $p\text{CO}_2$ (1,715 μatm) in the PRB was lower than the global median ($\sim 2,304$ μatm) (Stanley

et al., 2023). Consequently, the riverine CO_2 fluxes (median: $51 \text{ mmol m}^{-2} \text{ d}^{-1}$) measured through floating chambers were significantly lower than the global median value ($128 \text{ mmol m}^{-2} \text{ d}^{-1}$). In comparison, while the median $p\text{CH}_4$ ($289 \text{ } \mu\text{atm}$) was two times the global median value ($\sim 141 \text{ } \mu\text{atm}$), the corresponding diffusive CH_4 fluxes (median: $0.41 \text{ mmol m}^{-2} \text{ d}^{-1}$) were quite close to the global median ($0.44 \text{ mmol m}^{-2} \text{ d}^{-1}$) (Stanley et al., 2023). There are probably two reasons for the lower CO_2 concentrations and fluxes in the PRB compared to the global median. The observations in the global data set were primarily collected in summer when dissolved CO_2 concentrations and fluxes were high due to larger terrestrial carbon inputs into drainage networks (Liu et al., 2022; Stanley et al., 2023). Furthermore, the evasion of CO_2 in the PRB may have been substantially impacted by primary production in karst rivers, which resulted in a low evasion rate and even the lowest of all reported rivers worldwide (Zhang, Li, et al., 2017). This was further validated by the significant negative correlation between DO and $p\text{CO}_2$ ($R^2 = 0.68$, $p < 0.0001$), a relationship that is commonly interpreted as evidence for the crucial role of aquatic photosynthesis and respiration in regulating riverine CO_2 dynamics (e.g., Chen, Zhong, et al., 2021; Pu et al., 2017).

4.2. Hydrologic and Climatic Controls on CO_2 and CH_4 Concentrations and Fluxes

The seasonal $p\text{CO}_2$ and $p\text{CH}_4$ dynamics, as shown in Table 1, were likely linked to changes in water temperature, which was significantly different between the wet and dry seasons. The reduced gas solubility due to increased temperature in the wet season could lead to enhanced aquatic GHG evasion from surface waters (Dinsmore et al., 2013). In addition, the higher temperature in the wet season is an important factor in controlling riverine $p\text{CO}_2$ and $p\text{CH}_4$ dynamics by influencing aquatic primary productivity and respiration (Ludwig et al., 2022), promoting methanogenesis (Yvon-Durocher et al., 2014), and enhancing terrestrial microbial and vegetation productivity (Dinsmore et al., 2013), thereby resulting in higher GHG fluxes in the wet season. Particularly, the weak positive correlations between riverine $p\text{CO}_2$ and $p\text{CH}_4$ and water temperature (Figure 5) also suggest the temperature/climatic regulation on $p\text{CO}_2$ and $p\text{CH}_4$. Moreover, the seasonality of precipitation and subsequent changes in discharge and groundwater inflows are also significant determinants of the seasonal trends of GHG dynamics (Lupon et al., 2019), given the large seasonal variations in precipitation and discharge within the PRB (Han et al., 2018). We observed a significant positive correlation between runoff and $p\text{CO}_2$ ($p < 0.0001$; Figure S8a in Supporting Information S1). This is consistent with previous studies which demonstrate that increasing baseflow with large inputs of soil CO_2 in the early wet season can produce substantially higher $p\text{CO}_2$ in the Pearl River (Yao et al., 2007; Zhang et al., 2009). In addition, enhanced surface turbulence tends to increase gas transfer velocity (the k_{600} was significantly higher in the wet season than in the dry season, Table 1; $p < 0.01$, Mann-Whitney test), which, together with the higher $p\text{CO}_2$, led to the higher $F\text{CO}_2$ in the wet season (Table 1). The median $F\text{CO}_2$ was 445% higher in the wet season than in the dry season, revealing a significant difference in seasonal CO_2 emissions, which further highlights hydrology as a vital influencing factor in determining riverine $p\text{CO}_2$ dynamics (Liu et al., 2022; Marx et al., 2017).

Compared with the relatively weak impact of water temperature, $p\text{CO}_2$ and $p\text{CH}_4$ were strongly regulated by DO (Figures 5c and 5d), especially for CO_2 ($R^2 = 0.66$). DO is an essential indicator for river network metabolism (Battin et al., 2023), and it typically exerts a negative effect on riverine $p\text{CO}_2$ and $p\text{CH}_4$ (Borges et al., 2015; Ludwig et al., 2022). Aquatic photosynthesis and respiration produce and consume DO, respectively, with a low DO level denoting anoxic conditions favorable for methanogenesis (Anthony et al., 2012; Ludwig et al., 2022). The considerably higher DO levels during the dry season (Table 1) can be attributed to several factors. These include increased DO solubility resulting from cooler water temperature, reduced exchange with atmospheric oxygen owing to decreased water surface turbulence, and enhanced aquatic photosynthesis facilitated by low turbidity, high light transmissivity, and prolonged water retention in slowly flowing waters (Piatka et al., 2021). The higher DO levels in the dry season have likely contributed to the significantly lower $p\text{CH}_4$ due to the oxygenated environments, which are unsuitable for CH_4 production. Likewise, the enhanced aquatic photosynthesis with weakened microbial respiration in the dry season has also contributed to the lower $p\text{CO}_2$ (Campeau & Del Giorgio, 2014). Thus, both $p\text{CO}_2$ and $p\text{CH}_4$ and emission fluxes exhibited a strong seasonal variability in all rivers, with the median concentrations and fluxes in the wet season being two times higher than those in the dry season (Table 1). In short, DO and water temperature demonstrated the effects of stream metabolism, methanogenesis, and methane oxidation on CO_2 and CH_4 dynamics in the PRB.

Contrary to the temporal variation in CO_2 dynamics, seasonal changes in riverine CH_4 have rarely been reported worldwide. Prior studies have observed an inverse relationship between discharge and $p\text{CH}_4$ levels (e.g., Anthony

et al., 2012; Sawakuchi et al., 2014). This inverse relationship is largely attributed to a higher CH₄ evasion rate under high flow conditions due to enhanced surface turbulence, resulting in lower CH₄ concentrations in the river waters (Campeau & Del Giorgio, 2014). Additionally, the dilution of dissolved CH₄ by discharge (Anthony et al., 2012; Sawakuchi et al., 2014), and the limited CH₄ production due to the prolonged time of CH₄ oxidation in deeper water columns during high flow periods (Sawakuchi et al., 2014) can also contribute to this inverse relationship. However, Lupon et al. (2019) found a positive correlation between *p*CH₄ and discharge in a boreal stream, which was attributed to a greater groundwater CH₄ contribution during high-flow periods. Similarly, we discovered a significant increasing trend of *p*CH₄ with elevated runoff ($p < 0.0001$; Figure S8b in Supporting Information S1). However, when the riverine *p*CH₄ levels are exceptionally high (e.g., >2,000 μatm at some sites in the LJ catchment), its relationship with runoff no longer follows the positive correlation, which is probably due to anthropogenic influences (Figure S8b in Supporting Information S1). This suggests that a flow threshold may exist in controlling CH₄ production and evasion. Similar to CO₂, we observed a substantially higher diffusive CH₄ flux in the wet season than in the dry season (Table 1), which is in agreement with the considerably higher *p*CH₄ in the wet season than in the dry season. The driving mechanisms are consistent with the findings by Lupon et al. (2019), indicating the need for a higher sampling frequency to reduce the prediction error of CH₄ fluxes in river networks.

4.3. Differences Between Headspace-Based *p*CO₂ and Alkalinity-Based *p*CO₂

Previous studies on riverine *p*CO₂ in the Pearl River were largely determined by the indirect alkalinity-based method (e.g., Liu & Han, 2021; Zhang, Li, et al., 2017; Zhong et al., 2018). For karst rivers and streams, such as these in the Xijiang River basin, that are typically characterized by high ionic strength, high pH, and low DOC concentrations, the calculation errors of *p*CO₂ by this method are relatively low (Abril et al., 2015; Liu et al., 2020). However, it remains necessary to quantify the degree of accuracy of the estimated *p*CO₂ in these rivers to refine the flux estimates of riverine CO₂ emissions. Our study showed that the overall *p*CO₂ in the PRB is slightly underestimated (by 5%) if it is calculated by the alkalinity-based method. Nevertheless, this method can produce considerable overestimations (e.g., by 153% at site XJ3 in the mainstream of the Xijiang River) and underestimations (e.g., by 63% at site ZJ2 in the mainstream of the Beijiang River) at certain locations. In addition, approximately 30% of the modeled *p*CO₂ values exhibited an estimation error of more than 20%, which demonstrates that the alkalinity-based method is not applicable to the rivers in the Pearl River basin, even to the Xijiang River where karst rivers are widely distributed.

Based on the linear relationship between pH and the ratio between modeled to measured *p*CO₂, we further evaluated the most suitable pH range for using the alkalinity-based method. For estimation errors within 5% and 10%, the pH range was 7.38–7.79 and 7.17–8.00, respectively (Figure 6b). However, water samples with the pH ranging from 7.17 to 8.00 accounted for only 56% of the total in the PRB ($n = 124$), suggesting the difficulty of applying this technique to determine the riverine *p*CO₂. Moreover, it should be noted that in other rivers with low alkalinity and higher DOC concentrations (Abril et al., 2015; Liu et al., 2020), the *p*CO₂ errors from this approach will be even larger (e.g., +350% when total alkalinity <500 μmol L⁻¹; Abril et al., 2015) and the computed *p*CO₂ results are thus unreliable. Therefore, direct measurement of *p*CO₂ in most rivers using portable probes or the headspace equilibrium method is highly recommended to constrain the error to be <10%.

4.4. Regional and Global Significance of the Carbon Emissions From the PRB

The areal CO₂ fluxes in the PRB (mean: 790.1 mmol m⁻² d⁻¹) were higher than the global average of 594 mmol m⁻² d⁻¹ (Liu et al., 2022) and the temperate rivers of the conterminous United States (541 mmol m⁻² d⁻¹; Butman & Raymond, 2011), and even higher than tropical rivers (735 mmol m⁻² d⁻¹; Liu et al., 2022). Unexpectedly, the CO₂ fluxes (mean: 212 mmol m⁻² d⁻¹; Ran et al., 2021) in the Greater Pearl basin (a region including the PRB and adjacent subtropical rivers) estimated from water quality data were substantially lower than our results, further highlighting the significance of direct measurement of CO₂ emissions and the need for high-frequency sampling. In contrast to CO₂ fluxes, the mean diffusive CH₄ flux in the PRB (8.5 mmol m⁻² d⁻¹) was 2.5 times higher than the global mean diffusive flux (3.4 mmol m⁻² d⁻¹; Rocher-Ros et al., 2023), due largely to the warmer climate, high population densities, and strong river regulation, which are all common characteristics of (sub)tropical rivers (Park et al., 2018; Stanley et al., 2023). This suggests that current global significance of CH₄ emissions from subtropical river networks is probably underestimated (Rocher-Ros et al., 2023). The *F*CO₂/*F*CH₄ (diffusive CH₄ flux was expressed in CO₂-eq) ratios (mean: 3.1;

range: 1.8–4.9; Figure 7) in the PRB were significantly lower than previous studies in tropical rivers (e.g., 11; Borges et al., 2015), temperate rivers (e.g., 6–12; Galantini et al., 2021), alpine permafrost rivers (e.g., 23; Zhang et al., 2020), and high latitude rivers (e.g., 140; Striegl et al., 2012). The lower FCO_2/FCH_4 ratios in the PRB further challenge the conventional view that CH_4 emissions play a negligible role in GHG emissions from river ecosystems (Dahm et al., 1991), let alone the ebullitive CH_4 fluxes that were unaccounted for in this study. The unexpectedly lower ratios also reflect the higher CH_4 emission rates and the more widespread flooded areas in the PRB, which serve as hotspots for CH_4 production and emission (Borges et al., 2015). This is consistent with the spatial patterns of FCO_2 (a decreasing trend) and FCH_4 (no discernible trend) with the increasing stream order. Consequently, the flooded areas typically observed in high-order streams showed lower FCO_2/FCH_4 ratios.

For the entire PRB, low-order headwater streams (0–2) contributed to more than 70% of the total CO_2 and CH_4 emissions, suggesting the disproportionate role of headwater streams in basin-wide carbon emissions (Rocher-Ros et al., 2023). This also indicates that the spatial variability in diffusive CH_4 fluxes was mainly controlled by landscape-driven gas transfer velocity (i.e., k_{600}) given that pCH_4 was not significantly higher in low-order streams. Clearly, this is different from CO_2 emissions, with the pCO_2 in low-order streams significantly higher than that in high-order streams as discussed earlier, which is an important reason for the higher CO_2 fluxes in low-order streams. Yet, it must be pointed out that the higher gas transfer velocities in low-order streams are also crucial for maintaining their higher CO_2 fluxes (Butman & Raymond, 2011; Marx et al., 2017).

For the water surface area of the PRB, it is worth noting that the magnitude of its seasonal fluctuations is only 3.0%, similar to that in the Dongjiang River (Liu et al., 2023). This is probably because of the strong flow regulation resulting from dam operations in the PRB. Such regulation has remarkably reduced variations in stream width, which is an important factor influencing riverine carbon emissions yet rarely considered in previous studies. The substantially reduced flow velocity due to damming would further weaken water surface turbulence, leading to reduced gas transfer velocities and, subsequently, carbon emissions across the water-air interface (Ni et al., 2022). Therefore, the seasonal variations in basin-wide CO_2 and diffusive CH_4 fluxes were primarily regulated by seasonal changes in pCO_2 and pCH_4 as well as gas transfer velocities.

Undoubtedly, our basin-wide flux estimates of CO_2 and CH_4 emissions were likely conservative. First, our sampling sites are mostly located near watershed outlets with relatively gentle topography that is characterized by consistently lower flow velocities compared with upstream steep channels, resulting in distinctly lower k_{600} results than the values computed (Figure S9 in Supporting Information S1) using the models developed by Raymond et al. (2012). This finding aligns with prior studies conducted in the Yangtze River (Liu et al., 2017). This also explains why our estimated basin-wide emission rate (Section 3.4) holds greater global significance than the measured site-specific emission rate (Section 3.1). However, this is unavoidable in the study of large river systems because it is often challenging to perform in situ measurements at sites with steep slopes or under turbulent flow conditions (Borges et al., 2015; Liu et al., 2023). Second, ebullition is an important pathway for CH_4 emissions and the dominant pathway in some river systems (e.g., Aben et al., 2017; Crawford et al., 2014), especially in rivers with eutrophic environments (Park et al., 2023; Yang et al., 2024). For instance, ebullition can account for up to 99% of the total CH_4 flux in eutrophic urban rivers (Chen, Wang, et al., 2021). Similar to CO_2 fluxes, the inherent diel and seasonal variations in CH_4 ebullition further complicate flux estimation (Chen, Wang, et al., 2021; Sawakuchi et al., 2014). Due to the lack of reliable and widely applicable models in predicting the ebullitive CH_4 flux in large rivers, we did not quantify CH_4 ebullition in this study. Future research is needed to examine the spatiotemporal patterns of CH_4 ebullition and their underlying processes in the PRB. Furthermore, the use of floating chambers might be problematic by altering the natural state of flowing waters, leading to considerable errors in the computed areal emission rates (Campeau et al., 2014; Zheng et al., 2022). For large river basins such as the PRB, these errors may cause biases in flux upscaling due to the limited number of floating chamber deployments and the spatial heterogeneity in carbon emissions.

5. Conclusions

This research is the first study to analyze the spatial and temporal patterns in riverine CO_2 and CH_4 concentrations and emissions in the large subtropical monsoon Pearl River basin and to estimate the basin-wide CO_2 and diffusive CH_4 fluxes based on upscaling of in situ measurements across the PRB. Our results show a high spatial and temporal heterogeneity in both the concentrations and fluxes of riverine CO_2 and CH_4 , but with distinctive spatiotemporal patterns. There was a decreasing trend in pCO_2 and FCO_2 with increasing stream order, while

$p\text{CH}_4$ and $F\text{CH}_4$ displayed no discernible trend with stream order. Both dissolved CO_2 and CH_4 concentrations and fluxes were significantly higher in the wet season than in the dry season. Hydrology, water temperature, and DO were identified as primary regulators of the seasonal variations in $p\text{CO}_2$ and $p\text{CH}_4$, highlighting hydrologic and climatic controls on riverine GHG emissions, which have important biogeochemical implications in the context of global climate change. Based on basin-wide extrapolation, headwater streams (Strahler orders 0–2) contributed to 75% of the total emissions in terms of greenhouse warming potential. The areal CO_2 and diffusive CH_4 fluxes in the PRB are slightly higher (1.3 times) and significantly higher (2.5 times) than the global mean CO_2 and CH_4 fluxes, respectively. However, our flux estimates of the basin-wide GHG emissions are likely conservative due largely to their huge spatial and temporal heterogeneity. Further studies are warranted to integrate CH_4 ebullition into regional GHG emission estimates, which is probably a significant pathway of CH_4 emissions in subtropical rivers. This is particularly possible for river basins undergoing rapid urbanization and intensive agricultural activities. In addition, sampling with higher frequency in future upscaling efforts will certainly improve the basin-wide flux estimates.

Conflict of Interest

The authors declare no conflicts of interest relevant to this study.

Data Availability Statement

All data necessary to reproduce the reported finding are available at <https://doi.org/10.25442/hku.24548485>.

Acknowledgments

This work was supported financially by the Research Grants Council of Hong Kong (Grant 17300621) and the National Natural Science Foundation of China (Grants 42222062, 41925002, and 41422303).

References

- Aben, R. C. H., Barros, N., van Donk, E., Frenken, T., Hilt, S., Kazanjian, G., et al. (2017). Cross continental increase in methane ebullition under climate change. *Nature Communications*, 8(1), 1682. <https://doi.org/10.1038/s41467-017-01535-y>
- Abril, G., Bouillon, S., Darchambeau, F., Teodoru, C. R., Marwick, T. R., Tamoo, F., et al. (2015). Technical Note: Large overestimation of $p\text{CO}_2$ calculated from pH and alkalinity in acidic, organic-rich freshwaters. *Biogeosciences*, 12(1), 67–78. <https://doi.org/10.5194/bg-12-67-2015>
- Anthony, S. E., Prael, F. G., & Peterson, T. D. (2012). Methane dynamics in the Willamette River, Oregon. *Limnology & Oceanography*, 57(5), 1517–1530. <https://doi.org/10.4319/lo.2012.57.5.1517>
- Bastviken, D., Tranvik, L. J., Downing, J. A., Crill, P. M., & Enrich-Prast, A. (2011). Freshwater methane emissions offset the continental carbon sink. *Science*, 331(6013), 50. <https://doi.org/10.1126/science.1196808>
- Battin, T. J., Lauerwald, R., Bernhardt, E. S., Bertuzzo, E., Gener, L. G., Hall, R. O., Jr., et al. (2023). River ecosystem metabolism and carbon biogeochemistry in a changing world. *Nature*, 613(7944), 449–459. <https://doi.org/10.1038/s41586-022-05500-8>
- Borges, A. V., Darchambeau, F., Lambert, T., Morana, C., Allen, G. H., Tambwe, E., et al. (2019). Variations in dissolved greenhouse gases (CO_2 , CH_4 , N_2O) in the Congo River network overwhelmingly driven by fluvial-wetland connectivity. *Biogeosciences*, 16(19), 3801–3834. <https://doi.org/10.5194/bg-16-3801-2019>
- Borges, A. V., Darchambeau, F., Teodoru, C. R., Marwick, T. R., Tamoo, F., Geeraert, N., et al. (2015). Globally significant greenhouse-gas emissions from African inland waters. *Nature Geoscience*, 8(8), 637–642. <https://doi.org/10.1038/ngeo2486>
- Butman, D., & Raymond, P. A. (2011). Significant efflux of carbon dioxide from streams and rivers in the United States. *Nature Geoscience*, 4(12), 839–842. <https://doi.org/10.1038/ngeo1294>
- Campeau, A., & Del Giorgio, P. A. (2014). Patterns in CH_4 and CO_2 concentrations across boreal rivers: Major drivers and implications for fluvial greenhouse emissions under climate change scenarios. *Global Change Biology*, 20(4), 1075–1088. <https://doi.org/10.1111/gcb.12479>
- Campeau, A., Lapierre, J.-F., Vachon, D., & del Giorgio, P. A. (2014). Regional contribution of CO_2 and CH_4 fluxes from the fluvial network in a lowland boreal landscape of Québec. *Global Biogeochemical Cycles*, 28(1), 57–69. <https://doi.org/10.1002/2013gb004685>
- Chen, S., Wang, D., Ding, Y., Yu, Z., Liu, L., Li, Y., et al. (2021). Ebullition controls on CH_4 emissions in an urban, eutrophic river: A potential time-scale bias in determining the aquatic CH_4 flux. *Environmental Science & Technology*, 55(11), 7287–7298. <https://doi.org/10.1021/acs.est.1c00114>
- Chen, S., Zhong, J., Li, S., Ran, L., Wang, W., Xu, S., et al. (2021). Multiple controls on carbon dynamics in mixed karst and non-karst mountainous rivers, Southwest China, revealed by carbon isotopes ($\delta^{13}\text{C}$ and $\Delta^{14}\text{C}$). *Science of the Total Environment*, 791, 148347. <https://doi.org/10.1016/j.scitotenv.2021.148347>
- Ciais, P., Sabine, C., Bala, G., Bopp, L., Brovkin, V., Canadell, J., et al. (2014). In *Carbon and other biogeochemical cycles, paper presented at climate change 2013: The physical science basis. Contribution of working group I to the fifth assessment report of the intergovernmental panel on climate change*. Cambridge University Press.
- Crawford, J. T., Loken, L. C., West, W. E., Cray, B., Spawn, S. A., Gubbins, N., et al. (2017). Spatial heterogeneity of within-stream methane concentrations. *Journal of Geophysical Research: Biogeosciences*, 122(5), 1036–1048. <https://doi.org/10.1002/2016jg003698>
- Crawford, J. T., Stanley, E. H., Spawn, S. A., Finlay, J. C., Loken, L. C., & Striegl, R. G. (2014). Ebullitive methane emissions from oxygenated wetland streams. *Global Change Biology*, 20(11), 3408–3422. <https://doi.org/10.1111/gcb.12614>
- Dahm, C. N., Carr, D. L., & Coleman, R. L. (1991). Anaerobic carbon cycling in stream ecosystems. *Internationale Vereinigung für theoretische und angewandte Limnologie: Verhandlungen*, 24(3), 1600–1604. <https://doi.org/10.1080/03680770.1989.11899028>
- Dinsmore, K. J., Billett, M. F., & Dyson, K. E. (2013). Temperature and precipitation drive temporal variability in aquatic carbon and GHG concentrations and fluxes in a peatland catchment. *Global Change Biology*, 19(7), 2133–2148. <https://doi.org/10.1111/gcb.12209>
- Galantini, L., Lapierre, J.-F., & Maranger, R. (2021). How are greenhouse gases coupled across seasons in a large temperate river with differential land use? *Ecosystems*, 24(8), 2007–2027. <https://doi.org/10.1007/s10021-021-00629-5>

- Gómez-Gener, L., Siebers, A. R., Arce, M. I., Arnon, S., Bernal, S., Bolpagni, R., et al. (2021). Towards an improved understanding of biogeochemical processes across surface-groundwater interactions in intermittent rivers and ephemeral streams. *Earth-Science Reviews*, 220, 103724. <https://doi.org/10.1016/j.earscirev.2021.103724>
- Guo, X., Dai, M., Zhai, W., Cai, W. J., & Chen, B. (2009). CO₂ flux and seasonal variability in a large subtropical estuarine system, the Pearl River Estuary, China. *Journal of Geophysical Research*, 114(G3), G03013. <https://doi.org/10.1029/2008jg000905>
- Han, G., Lv, P., Tang, Y., & Song, Z. (2018). Spatial and temporal variation of H and O isotopic compositions of the Xijiang River system, Southwest China. *Isotopes in Environmental and Health Studies*, 54(2), 137–146. <https://doi.org/10.1080/10256016.2017.1368507>
- Hutchins, R. H. S., Prairie, Y. T., & del Giorgio, P. A. (2019). Large-scale landscape drivers of CO₂, CH₄, DOC, and DIC in boreal river networks. *Global Biogeochemical Cycles*, 33(2), 125–142. <https://doi.org/10.1029/2018gb006106>
- Koschorreck, M., Prairie, Y. T., Kim, J., & Marcé, R. (2021). Technical note: CO₂ is not like CH₄—Limits of and corrections to the headspace method to analyse CO₂ in fresh water. *Biogeosciences*, 18(5), 1619–1627. <https://doi.org/10.5194/bg-18-1619-2021>
- Linke, S., Lehner, B., Ouellet Dallaire, C., Ariwi, J., Grill, G., Anand, M., et al. (2019). Global hydro-environmental sub-basin and river reach characteristics at high spatial resolution. *Scientific Data*, 6(1), 283. <https://doi.org/10.1038/s41597-019-0300-6>
- Liu, B., Tian, M., Shih, K., Chan, C. N., Yang, X., & Ran, L. (2021). Spatial and temporal variability of CO₂ and CO₂ emissions from the Dong River in south China. *Biogeosciences*, 18(18), 5231–5245. <https://doi.org/10.5194/bg-18-5231-2021>
- Liu, B., Wang, Z., Tian, M., Yang, X., Chan, C. N., Chen, S., et al. (2023). Basin-scale CO₂ emissions from the East River in South China: Importance of small rivers, human impacts and monsoons. *Journal of Geophysical Research: Biogeosciences*, 128(1), e2022JG007291. <https://doi.org/10.1029/2022jg007291>
- Liu, J., & Han, G. (2021). Controlling factors of riverine CO₂ partial pressure and CO₂ outgassing in a large karst river under base flow condition. *Journal of Hydrology*, 593, 125638. <https://doi.org/10.1016/j.jhydrol.2020.125638>
- Liu, S., Butman, D. E., & Raymond, P. A. (2020). Evaluating CO₂ calculation error from organic alkalinity and pH measurement error in low ionic strength freshwaters. *Limnology and Oceanography: Methods*, 18(10), 606–622. <https://doi.org/10.1002/lom3.10388>
- Liu, S., Kuhn, C., Amatulli, G., Aho, K., Butman, D. E., Allen, G. H., et al. (2022). The importance of hydrology in routing terrestrial carbon to the atmosphere via global streams and rivers. *Proceedings of the National Academy of Sciences of the United States of America*, 119(11), e2106322119. <https://doi.org/10.1073/pnas.2106322119>
- Liu, S., Lu, X. X., Xia, X., Yang, X., & Ran, L. (2017). Hydrological and geomorphological control on CO₂ outgassing from low-gradient large rivers: An example of the Yangtze River system. *Journal of Hydrology*, 550, 26–41. <https://doi.org/10.1016/j.jhydrol.2017.04.044>
- Ludwig, S. M., Natali, S. M., Mann, P. J., Schade, J. D., Holmes, R. M., Powell, M., et al. (2022). Using machine learning to predict inland aquatic CO₂ and CH₄ concentrations and the effects of Wildfires in the Yukon-Kuskokwim delta, Alaska. *Global Biogeochemical Cycles*, 36(4). <https://doi.org/10.1029/2021gb007146>
- Lupon, A., Denfeld, B. A., Laudon, H., Leach, J., Karlsson, J., & Sponseller, R. A. (2019). Groundwater inflows control patterns and sources of greenhouse gas emissions from streams. *Limnology & Oceanography*, 64(4), 1545–1557. <https://doi.org/10.1002/lno.11134>
- Marx, A., Dusek, J., Jankovec, J., Sanda, M., Vogel, T., van Geldern, R., et al. (2017). A review of CO₂ and associated carbon dynamics in headwater streams: A global perspective. *Reviews of Geophysics*, 55(2), 560–585. <https://doi.org/10.1002/2016RG000547>
- NASA, METI, AIST, Spacesystems, J., & Team, U. S. J. A. S. (2018). ASTER global digital elevation model V003 [Dataset]. *NASA EOSDIS Land Processes Distributed Active Archive Center*. <https://doi.org/10.5067/ASTER/ASTGTM.003>
- Nayna, O. K., Begum, M. S., Ran, L., & Park, J.-H. (2021). Improving carbonate equilibria-based estimation of pCO₂ in anthropogenically impacted river systems. *Frontiers in Earth Science*, 9. <https://doi.org/10.3389/feart.2021.778215>
- Ni, J., Wang, H., Ma, T., Huang, R., Ciais, P., Li, Z., et al. (2022). Three Gorges Dam: Friend or foe of riverine greenhouse gases? *National Science Review*, 9(6), nwac013. <https://doi.org/10.1093/nsr/nwac013>
- Park, J.-H., Lee, H., Zhumabieke, M., Kim, S.-H., Shin, K.-H., & Khim, B.-K. (2023). Basin-specific pollution and impoundment effects on greenhouse gas distributions in three rivers and estuaries. *Water Research*, 236, 119982. <https://doi.org/10.1016/j.watres.2023.119982>
- Park, J.-H., Nayna, O. K., Begum, M. S., Chea, E., Hartmann, J., Keil, R. G., et al. (2018). Reviews and syntheses: Anthropogenic perturbations to carbon fluxes in Asian river systems – Concepts, emerging trends, and research challenges. *Biogeosciences*, 15(9), 3049–3069. <https://doi.org/10.5194/bg-15-3049-2018>
- Parkhurst, D. L., & Appelo, C. (2013). *Description of input and examples for PHREEQC version 3: A computer program for speciation, batch-reaction, one-dimensional transport, and inverse geochemical calculations*. Rep (pp. 2328–7055). US Geological Survey.
- Piatka, D. R., Wild, R., Hartmann, J., Kaule, R., Kaule, L., Gilfedder, B., et al. (2021). Transfer and transformations of oxygen in rivers as catchment reflectors of continental landscapes: A review. *Earth-Science Reviews*, 220, 103729. <https://doi.org/10.1016/j.earscirev.2021.103729>
- Pu, J., Li, J., Khadka, M. B., Martin, J. B., Zhang, T., Yu, S., & Yuan, D. (2017). In-stream metabolism and atmospheric carbon sequestration in a groundwater-fed karst stream. *Science of the Total Environment*, 579, 1343–1355. <https://doi.org/10.1016/j.scitotenv.2016.11.132>
- Ran, L., Butman, D. E., Battin, T. J., Yang, X., Tian, M., Duvert, C., et al. (2021). Substantial decrease in CO₂ emissions from Chinese inland waters due to global change. *Nature Communications*, 12(1), 1730. <https://doi.org/10.1038/s41467-021-21926-6>
- Ran, L., Lu, X. X., & Liu, S. (2017). Dynamics of riverine CO₂ in the Yangtze River fluvial network and their implications for carbon evasion. *Biogeosciences*, 14(8), 2183–2198. <https://doi.org/10.5194/bg-14-2183-2017>
- Raymond, P. A., Hartmann, J., Lauerwald, R., Sobek, S., McDonald, C., Hoover, M., et al. (2013). Global carbon dioxide emissions from inland waters. *Nature*, 503(7476), 355–359. <https://doi.org/10.1038/nature12760>
- Raymond, P. A., Zappa, C. J., Butman, D., Bott, T. L., Potter, J., Mulholland, P., et al. (2012). Scaling the gas transfer velocity and hydraulic geometry in streams and small rivers. *Limnology and Oceanography: Fluids and Environments*, 2(1), 41–53. <https://doi.org/10.1215/21573689-1597669>
- Regnier, P., Resplandy, L., Najjar, R. G., & Ciais, P. (2022). The land-to-ocean loops of the global carbon cycle. *Nature*, 603(7901), 401–410. <https://doi.org/10.1038/s41586-021-04339-9>
- Rocher-Ros, G., Stanley, E. H., Loken, L. C., Casson, N. J., Raymond, P. A., Liu, S., et al. (2023). Global methane emissions from rivers and streams. *Nature*, 621(7979), 530–535. <https://doi.org/10.1038/s41586-023-06344-6>
- Sawakuchi, H. O., Bastviken, D., Sawakuchi, A. O., Krusche, A. V., Ballester, M. V., & Richey, J. E. (2014). Methane emissions from Amazonian Rivers and their contribution to the global methane budget. *Global Change Biology*, 20(9), 2829–2840. <https://doi.org/10.1111/gcb.12646>
- Stanley, E. H., Casson, N. J., Christel, S. T., Crawford, J. T., Loken, L. C., & Oliver, S. K. (2016). The ecology of methane in streams and rivers: Patterns, controls, and global significance. *Ecological Monographs*, 86(2), 146–171. <https://doi.org/10.1890/15-1027>
- Stanley, E. H., Loken, L. C., Casson, N. J., Oliver, S. K., Sponseller, R. A., Wallin, M. B., et al. (2023). GRiMeDB: The global river methane database of concentrations and fluxes. *Earth System Science Data*, 15(7), 2879–2926. <https://doi.org/10.5194/essd-15-2879-2023>

- Stets, E. G., Butman, D., McDonald, C. P., Stackpoole, S. M., DeGrandpre, M. D., & Striegl, R. G. (2017). Carbonate buffering and metabolic controls on carbon dioxide in rivers. *Global Biogeochemical Cycles*, *31*(4), 663–677. <https://doi.org/10.1002/2016gb005578>
- Striegl, R. G., Dornblaser, M. M., McDonald, C. P., Rover, J. R., & Stets, E. G. (2012). Carbon dioxide and methane emissions from the Yukon River system. *Global Biogeochemical Cycles*, *26*(4). <https://doi.org/10.1029/2012gb004306>
- Tang, W., Xu, Y. J., Ma, Y., Maher, D. T., & Li, S. (2021). Hot spot of CH₄ production and diffusive flux in rivers with high urbanization. *Water Research*, *204*, 117624. <https://doi.org/10.1016/j.watres.2021.117624>
- Valentine, P. C. (2019). *Sediment classification and the characterization, identification, and mapping of geologic substrates for the glaciated Gulf of Maine seabed and other terrains, providing a physical framework for ecological research and seabed management*. Rep. 2328-0328. US Geological Survey.
- Yang, Q., Chen, S., Li, Y., Liu, B., & Ran, L. (2024). Carbon emissions from Chinese inland waters: Current progress and future challenges. *Journal of Geophysical Research: Biogeosciences*, *129*(2). <https://doi.org/10.1029/2023jg007675>
- Yao, G., Gao, Q., Wang, Z., Huang, X., Tong, H. E., Zhang, Y., et al. (2007). Dynamics of CO₂ partial pressure and CO₂ outgassing in the lower reaches of the Xijiang River, a subtropical monsoon river in China. *Science of the Total Environment*, *376*(1), 255–266. <https://doi.org/10.1016/j.scitotenv.2007.01.080>
- Ye, W., Zhang, G., Zheng, W., Zhang, H., & Wu, Y. (2019). Methane distributions and sea-to-air fluxes in the Pearl River Estuary and the northern South China Sea. *Deep Sea Research Part II: Topical Studies in Oceanography*, *167*, 34–45. <https://doi.org/10.1016/j.dsr2.2019.06.016>
- Yvon-Durocher, G., Allen, A. P., Bastviken, D., Conrad, R., Gudasz, C., St-Pierre, A., et al. (2014). Methane fluxes show consistent temperature dependence across microbial to ecosystem scales. *Nature*, *507*(7493), 488–491. <https://doi.org/10.1038/nature13164>
- Zhang, L., Xia, X., Liu, S., Zhang, S., Li, S., Wang, J., et al. (2020). Significant methane ebullition from alpine permafrost rivers on the East Qinghai–Tibet Plateau. *Nature Geoscience*, *13*(5), 349–354. <https://doi.org/10.1038/s41561-020-0571-8>
- Zhang, S., Lu, X. X., Sun, H., Han, J., & Higgitt, D. L. (2009). Major ion chemistry and dissolved inorganic carbon cycling in a human-disturbed mountainous river (the Luodingjiang River) of the Zhujiang (Pearl River), China. *Science of the Total Environment*, *407*(8), 2796–2807. <https://doi.org/10.1016/j.scitotenv.2008.12.036>
- Zhang, T., Li, J., Pu, J., Martin, J. B., Khadka, M. B., Wu, F., et al. (2017). River sequesters atmospheric carbon and limits the CO₂ degassing in karst area, southwest China. *Science of the Total Environment*, *609*, 92–101. <https://doi.org/10.1016/j.scitotenv.2017.07.143>
- Zhang, T., Li, J., Pu, J., & Wu, F. (2021). Physical and chemical control on CO₂ gas transfer velocities from a low-gradient subtropical stream. *Water Research*, *204*, 117564. <https://doi.org/10.1016/j.watres.2021.117564>
- Zhang, Z., Zimmermann, N. E., Stenke, A., Li, X., Hodson, E. L., Zhu, G., et al. (2017). Emerging role of wetland methane emissions in driving 21st century climate change. *Proceedings of the National Academy of Sciences of the United States of America*, *114*(36), 9647–9652. <https://doi.org/10.1073/pnas.1618765114>
- Zheng, Y., Wu, S., Xiao, S., Yu, K., Fang, X., Xia, L., et al. (2022). Global methane and nitrous oxide emissions from inland waters and estuaries. *Global Change Biology*, *28*(15), 4713–4725. <https://doi.org/10.1111/gcb.16233>
- Zhong, J., Li, S.-L., Liu, J., Ding, H., Sun, X., Xu, S., et al. (2018). Climate variability controls on CO₂ consumption fluxes and carbon dynamics for monsoonal rivers: Evidence from Xijiang River, southwest China. *Journal of Geophysical Research: Biogeosciences*, *123*(8), 2553–2567. <https://doi.org/10.1029/2018JG004439>
- Zhu, Y., Jones, J. I., Collins, A. L., Zhang, Y., Olde, L., Rovelli, L., et al. (2022). Separating natural from human enhanced methane emissions in headwater streams. *Nature Communications*, *13*(1), 3810. <https://doi.org/10.1038/s41467-022-31559-y>

References From the Supporting Information

- Barbosa, P. M., Melack, J. M., Farjalla, V. F., Amaral, J. H. F., Scofield, V., & Forsberg, B. R. (2016). Diffusive methane fluxes from Negro, Solimões and Madeira rivers and fringing lakes in the Amazon basin. *Limnology & Oceanography*, *61*(S1), S221–S237. <https://doi.org/10.1002/lno.10358>
- Gong, P., Liu, H., Zhang, M., Li, C., Wang, J., Huang, H., et al. (2019). Stable classification with limited sample: Transferring a 30-m resolution sample set collected in 2015 to mapping 10-m resolution global land cover in 2017. *Science Bulletin*, *64*(6), 370–373. <https://doi.org/10.1016/j.scib.2019.03.002>
- Hartmann, J., & Moosdorf, N. (2012). The new global lithological map database GLiM: A representation of rock properties at the earth surface. *Geochemistry, Geophysics, Geosystems*, *13*(12), Q12004. <https://doi.org/10.1029/2012gc004370>
- Robinson, N., Regetz, J., & Guralnick, R. P. (2014). EarthEnv-DEM90: A nearly-global, void-free, multi-scale smoothed, 90m digital elevation model from fused ASTER and SRTM data. *ISPRS Journal of Photogrammetry and Remote Sensing*, *87*, 57–67. <https://doi.org/10.1016/j.isprsjprs.2013.11.002>
- Sujud, L. H., & Jaafar, H. H. (2022). A global dynamic runoff application and dataset based on the assimilation of GPM, SMAP, and GCN250 curve number datasets. *Scientific Data*, *9*(1), 706. <https://doi.org/10.1038/s41597-022-01834-0>
- Warszawski, L., Frieler, K., Huber, V., Piontek, F., Serdeczny, O., Zhang, X., et al. (2017). Center for international earth science information network—Ciesin—Columbia University. (2016). Gridded population of the world, version 4 (GPWV4): Population density. Palisades, NY. In *NASA socioeconomic data and applications center (SEDAC), Atlas of environmental risks facing China under climate change*. (p. 228). <https://doi.org/10.7927/h4np22dq>